CHALLENGES IN ELECTRON BEAM DIAGNOSTICS WITH TURBO-ICT AT PETAWATT-CLASS LASER FACILITIES

V. L. J. Phung*, M. Gugiu†, Y. Nakamiya, S. Tazlauanu, D. Doria, P. Ghenuche, O. Tesileanu,
Extreme Light Infrastructure - Nuclear Physics, Horia Hulubei National Institute for R&D in Physics and Nuclear Engineering, Magurele-Ilfov, Romania

Abstract

Laser–plasma acceleration (LPA) produces high-energy electron beams but faces severe shot-to-shot charge measurement challenges due to intense laser-driven electromagnetic pulses (EMPs). At the ELI-NP laser facility, a Turbo-Integrating Current Transformer (Turbo-ICT) system used for non-interceptive charge diagnostics during laser wakefield acceleration (LWFA) experienced significant signal distortion and parasitic coupling from this broadband EMP interference. The EMP environment was characterised using Moebius-loop antennas operating up to the GHz range. To improve diagnostic robustness, a comprehensive mitigation strategy was validated, combining enhanced shielding, optimised routing, spatial separation, and offline signal reconstruction. This methodology establishes a robust framework for reliable, online beam diagnostics in next-generation, high-repetition-rate LPA facilities operating under extreme electromagnetic conditions.

INTRODUCTION

In laser wakefield acceleration experiments, reliable shot-to-shot beam diagnostics are critical for evaluating acceleration performance and ensuring stable operation under high-repetition-rate conditions. Among the key beam parameters, the electron bunch charge is commonly measured using Integrating Current Transformers (ICTs), due to their non-interceptive operation, high sensitivity, and vacuum compatibility. However, in petawatt-class laser facilities, the interaction of ultra-intense laser pulses with matter generates severe electromagnetic interference (EMI) capable of perturbing sensitive diagnostics and acquisition electronics.

At the ELI-NP facility [1], EMP-induced perturbations affecting the Turbo-ICT and BCM-RF-E electronics were systematically observed during experiments, introducing significant uncertainties into the charge reconstruction. To address this, EMP measurements were performed using Moebius-loop antennas deployed both inside and outside the interaction chamber to characterise the EMP environment and identify dominant coupling mechanisms. The resulting data demonstrate that EMP coupling does not merely introduce stochastic noise into the acquisition chain but systematically alters the reconstructed charge response of the Turbo-ICT system under petawatt-class operating conditions. Consequently, a dedicated EMC mitigation strategy was implemented and experimentally validated, significantly improving diagnostic reliability.

* vanessa.phung@eli-np.ro
† marius.gugiu@eli-np.ro

EXPERIMENTAL ARRANGEMENT

Overview

The LWFA experiment utilises the high-power laser system (HPLS) focused onto a pulsed-solenoid gas jet by an $f/18$, 4.5° off-axis parabolic (OAP) mirror, yielding a 19 µm FWHM focal spot diameter [2]. The gas jet operates with variable backing pressure and is triggered via a TTL signal synchronised with laser arrival [3]. The E7 experimental area constitutes a fully enclosed environment providing radiological protection and electromagnetic shielding exceeding 60 dB in the 10 MHz–10 GHz frequency range. Several diagnostic configurations were investigated, with positions labelled "A1–A6" corresponding to different setups during the beamtime. In Fig. 1, the *blue-shaded* region indicates the location of the C3 vacuum chamber, which is subsequently removed to allow installation of the Turbo-ICT at position A4, outside the interaction chamber in air. An EMP monitoring system [4], positioned outside the experimental area and based exclusively on Moebius-loop antennas [5], is employed.

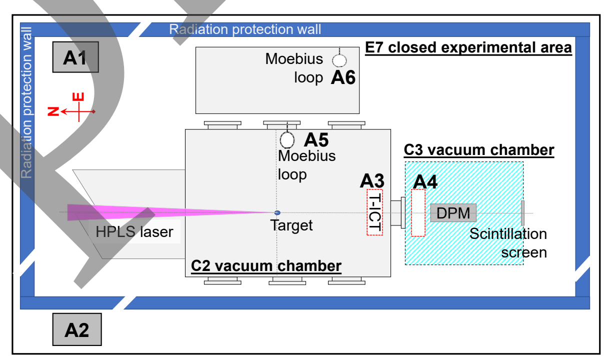

Figure 1: Detailed schematic of the E7 experimental setup. The layout shows the laser propagation through the vacuum chambers to the target and the respective positions (A1–A6).

Beam Charge Diagnostics

The Turbo-ICT (Turbo-ICT-VAC-082, Bergoz Instrumentation) current sensor and beam current monitor (BCM-RF-E) electronics receiver in Fig. 2 provide non-interceptive bunch-charge and average-current measurements with high sensitivity and low intrinsic noise [6]. The intense EMP environment can induce transient signal distortion and compromise sensitive electronics. In this work, the Turbo-ICT was connected to the BCM-RF-E and a 1 GHz bandwidth oscilloscope (Tektronix MSO5) via SMA-SMA semi-rigid coaxial cable (Huber+Suhner Sucoform-141-Cu). The acquisition electronics were installed inside a shielded enclosure with remote network accessibility to minimise direct EMP exposure. In order to improve the reliability of the

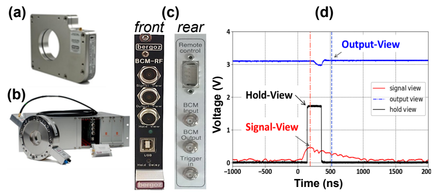

Figure 2: Components of the charge measurement system: (a) Turbo-ICT sensor, (b) BCM-RF-E electronics system from Bergoz Instrumentation [6], and (c) front/rear interface panels. (d) Representative oscilloscope traces of the *"Signal-View"*, *"Hold-View"*, and *"Output-View"* signals.

data acquisition, the Turbo-ICT and BCM-RF-E system were calibrated with the Remote Attenuation Module (RATT) before installation in the ELI-NP experimental area. Subsequently, the beam charge was reconstructed offline from the acquired experimental waveforms by extracting the peak value $V_{\text{sig, peak}}$ and the background level V_{BG} from the BCM-RF-E "*Signal-View*" signal, as shown in Fig. 2(d). The calibration procedure is described by Eq. (1) and Eq. (2).

$$Q_{\text{fit\_sig\_RATT}}[\text{pC}] = Q_{\text{cal}} \times 10^{V_{\text{BCM}}/U_{\text{cal}}} \quad (1)$$

$$V_{\text{BCM}}[\text{V}] = 7.96 \times (V_{\text{sig,peak}} - V_{\text{BG}}) - 0.15 \quad (2)$$

where the calibration constants are $Q_{\text{cal}} = 0.24975$ and $U_{\text{cal}} = 0.86478$. According to the manual [6], the timing synchronisation of the BCM-RF-E receiver is important. The rising edge of the *"Hold-View"* must overlap the apex of the *"Signal-View"* to capture the peak value converted into the *"Output-View"* (V_{BCM}) used by the GUI for charge calculation. However, in our experiment, EMP-induced perturbations introduced timing uncertainties into the acquisition process, motivating the implementation of a dedicated EMP mitigation strategy.

EMP Monitoring System

The EMP generated during the laser–plasma interaction was monitored using the *in-house* EMP monitoring system [4] via two broadband Moebius-loop probes acting as magnetic-field sensors. Inside the chamber, a 12.5 mm diameter probe (M12.5) in Fig. 3, was placed 20 cm from the eastern wall to measure the horizontal North–South magnetic field. Outside, an 8 mm diameter probe was positioned 1.5 m from the same wall along the East–West direction to measure the attenuated EMP field outside the interaction chamber. Low-loss coaxial cables routed the signals to a 1 GHz oscilloscope outside the E7 area, co-located with the BCM-RF-E electronics in a rack providing approximately 60 dB shielding from 10 MHz to 10 GHz. Recorded voltages were post-processed using the full system transfer function to reconstruct the magnetic field waveform $H(t)$ and its spectrum, enabling direct evaluation of shielding effectiveness and dominant coupling paths.

RESULTS AND DATA ANALYSIS

The electromagnetic pulse generated during the laser–plasma interaction was investigated to evaluate its impact on the operational reliability of the Turbo-ICT charge diagnostic system. Simultaneous measurements were

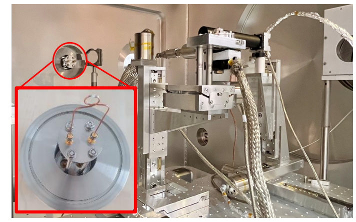

Figure 3: Moebius-loop antenna probe (M12.5) mounted on a DN16 flange inside the C2 vacuum chamber. *Inset*: enlarged view of the Moebius-loop antenna.

performed inside and outside the interaction chamber using Moebius-loop antennas. The measured voltage signals were corrected using the complete system transfer function of the antenna and acquisition chain in order to reconstruct the magnetic field waveform $H(t)$ and its corresponding frequency spectrum according to Eq. (3). Consequently, the EMP results are presented in terms of magnetic field intensity (A/m) rather than raw voltage signals.

$$H(f) = \frac{V_{\text{meas}}(f)}{T_{\text{sys}}(f)} \quad (3)$$

For an approximate estimation of the associated electric field amplitude, the local plane-wave relation $E(t) \approx Z_0 H(t)$ was considered, where $Z_0 \approx 377\ \Omega$ represents the free-space impedance. Reconstructed peak-to-peak electric field amplitudes inside the chamber reached up to approximately 150 kV/m, with corresponding magnetic field amplitudes approaching 400 A/m, confirming EMP levels sufficiently high to perturb sensitive diagnostics and acquisition electronics. Figure 4 presents representative reconstructed magnetic field waveforms measured inside and outside the interaction chamber. The interior waveform exhibits a high-amplitude transient followed by damped oscillations associated with cavity resonances and multiple reflections, whereas the exterior signal shows significantly reduced amplitude due to shielding attenuation. Figure 5 presents the corrected Fast Fourier Transform (FFT) spectra of the reconstructed magnetic fields. The interior spectrum exhibits a broadband response extending from approximately 80 MHz up to nearly 1 GHz, with dominant spectral components concentrated below approximately 400 MHz. In contrast, the exterior spectrum appears attenuated and spectrally modified, reflecting shielding attenuation and electromagnetic leakage paths.

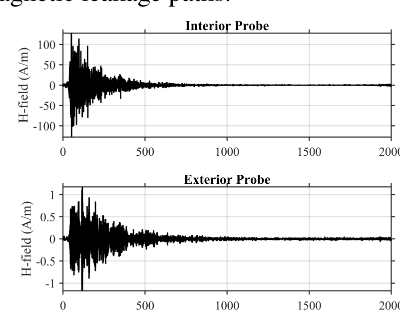

Figure 4: Reconstructed magnetic field $H(t)$ at the probe head.

Figure 6 compares the raw *"Signal-View"* data obtained for two distinct experimental configurations: (i) an

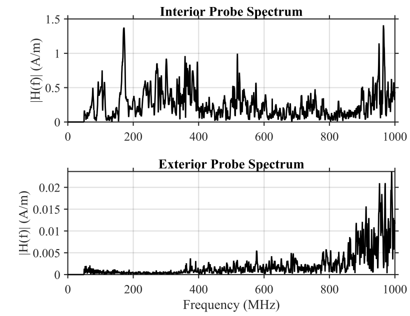

Figure 5: Spectral characterisation of EMP magnetic fields inside the interaction chamber and in the experimental area using a Moebius antenna.

EMP-exposed configuration, with the Turbo-ICT (A3) mounted inside the vacuum chamber (≈ 60 cm from the target) and its associated electronics located in enclosure A1 within the E7 experimental hall; and (ii) a *shielded/attenuated configuration*, where the Turbo-ICT (A4) is positioned outside the chamber (≈ 90 cm from the target) and the electronics are relocated to enclosure A2 outside the E7 hall. This latter configuration benefits from both the increased spatial separation and the inherent electromagnetic attenuation provided by the chamber walls and external housing, thereby reducing EMP-induced coupling and improving signal integrity, as evidenced by the suppression of transient overvoltage spikes. These results demonstrate the effectiveness of the implemented EMP mitigation strategy and are in good agreement with the observations presented in Figs. 4 and 5, where the EMP amplitude is also significantly suppressed. Overall, this configuration represents a major improvement to the charge diagnostic system in the E7/1PW area. By exploiting the natural shielding provided by the interaction chamber walls and the external enclosure, transient overvoltage spikes are effectively minimised. Under the experimental conditions

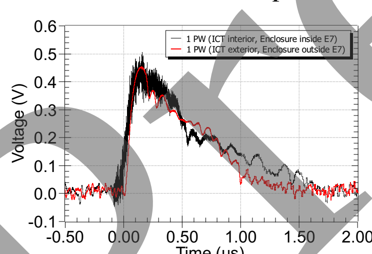

Figure 6: Raw *"Signal-View"* data recorded at the E7/1PW area. The Turbo-ICT was placed inside the interaction chamber with the BCM-RF-E unit inside the E7 area (*red solid line*), compared to both devices placed outside the chamber and E7 area (*black solid line*).

investigated in this work, EMP-induced transient overvoltage spikes were found to distort the *"Signal-View"* response of the BCM-RF-E electronics, leading to charge overestimation when standard processing routines are applied. To mitigate these effects, an EMP mitigation strategy combining offline signal processing, improved shielding, optimised cable routing, and increased spatial separation from the interaction region was implemented. Figure 7 shows that the in-chamber EMP amplitude tracks the shot-to-shot dynamics and clearly correlates with the measured electron beam charge. This

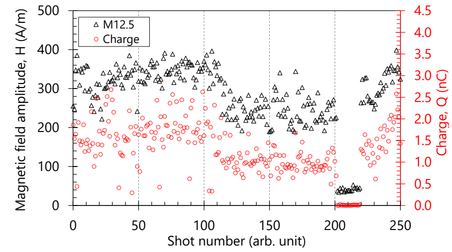

Figure 7: Correlation between charge (*red circle*) and magnetic field amplitude measured inside the interaction chamber using the Moebius-loop antenna M12.5 (*black triangle*) on a shot-by-shot basis, showing the synchronised behaviour of the two diagnostics.

behaviour is physically consistent, as a larger charge and current generation during the interaction lead to stronger EMP emission. However, even when no significant electron beam is observed (e.g., shots 200–220), persistent EMP activity remains detectable. This indicates that EMP generation is not exclusively driven by the accelerated electron beam itself, but by the overall laser–plasma interaction dynamics. These observations underscore that insufficient shielding of the diagnostic chain can directly compromise the reliability of charge reconstruction in petawatt-class laser experiments.

CONCLUSION

This work investigated the impact of laser-driven electromagnetic pulses (EMPs) on Turbo-ICT charge diagnostics during petawatt-class experiments at ELI-NP. In-chamber measurements revealed an extreme, broadband EMP environment up to 1 GHz (with dominant spectral energy below approximately 400 MHz) featuring magnetic fields reaching several hundred A/m and electric fields approaching 100 kV/m. Radiative and conductive EMP coupling directly perturbs the BCM-RF-E acquisition chain and distorts the *"Signal-View"* response, introducing systematic uncertainties rather than simple stochastic noise. To improve diagnostic robustness, a validated electromagnetic compatibility (EMC) strategy was implemented, combining enhanced shielding, Faraday enclosures, optimised routing, spatial separation, and offline signal reconstruction. This methodology establishes a robust framework for reliable online diagnostics in future high-repetition-rate, ultra-intense laser facilities.

ACKNOWLEDGEMENTS

This work is supported by Romanian Ministry of Education and Research through contract PN23210105, ELI-RO/RDI/2024-040, ELI-RO/RDI/2024-021, ELI-RO /DEZ/2023-001, ELI-NP Phase 2 ERDF/COP(1/07.07.2016, ID1334), and IOSIN-ELI. The authors also thank their colleagues for technical support during the experiments.

REFERENCES

[1] K. Tanaka *et al.*, "Current status and highlights of the ELI-NP research program", *Matter Radiat. Extrem.*, vol. 5, p. 024402, Mar. 2020. doi:10.1063/1.5093535

[2] Y. Nakamiya *et al.*, "Implementation of 1PW optical system for long-focal experiments at E7 area", in *ELI-NP Annual Report 2022–2024*. Extreme Light Infrastructure - Nuclear Physics, 2024, pp. 112–113. https://www.eli-np.ro/documents/ELI-NP-Annual_Report-2022-2024.pdf

[3] V. L. J. Phung *et al.*, "Gas density measurement for the 1 mm diameter "in-house" conical nozzle", in *ELI-NP Annual Report 2022–2024*. Extreme Light Infrastructure - Nuclear Physics, 2024, pp. 115–116. https://www.eli-np.ro/documents/ELI-NP-Annual_Report-2022-2024.pdf

[4] M. Gugiu *et al.*, "Monitoring system for electromagnetic pulses at ELI-NP", in *ELI-NP Annual Report 2020–2021*. Extreme Light Infrastructure - Nuclear Physics, 2021, pp. 141–144. https://www.eli-np.ro/documents/ELI-NP-Annual_Report-2020-2021.pdf

[5] P. H. Duncan, "Analysis of the moebius loop magnetic field sensor", *IEEE Trans. Electromagn. Compat.*, vol. EMC-16, no. 2, pp. 83–89, 1974. doi:10.1109/TEMC.1974.303336

[6] Bergoz Instrumentation, *Turbo-ICT & BCM-RF-E: user's manual*. Saint Genis Pouilly, Saint Genis Pouilly, France: Bergoz Instrumentation, France, 2019. https://www.bergoz.com/products/turbo-ict/